Hindawi
Advances in Civil Engineering
Volume 2022, Article ID 5297864, 18 pages
https://doi.org/10.1155/2022/5297864

Research Article

Finite Element and Vulnerability Analyses of a Building Failure due to Landslide in Kaithakunda, Kerala, India

Rajkumar Andrewwinner[1] and Sembulichampalayam Sennimalai Chandrasekaran[2]

[1]*Department of Structural and Geotechnical Engineering, School of Civil Engineering, Vellore Institute of Technology, Vellore, Tamil Nadu 632014, India*
[2]*Centre for Disaster Mitigation and Management (CDMM), Vellore Institute of Technology, Vellore, Tamil Nadu 632014, India*

Correspondence should be addressed to Sembulichampalayam Sennimalai Chandrasekaran; chandrasekaran.ss@vit.ac.in

Received 3 December 2021; Accepted 23 February 2022; Published 17 March 2022

Academic Editor: Ravindran Gobinath

Rainfall-induced landslide is one of the major natural disasters in the Western Ghats of India. Kerala state in southern India received unprecedented heavy rainfall from July to August 2018. The rainfall received was higher than the average for the past 100 years. The present study discusses the investigation of vertical cut failure at Kaithakunda, located in Malappuram district, Kerala, India. It was due to the series of medium rainfall followed by a short period of extremely heavy rainfall. The heavy rainfall triggered the slope failure, which led to the damage of the building and the death of three residents of the building. The index and engineering properties of the soil were evaluated from the laboratory tests. The tests revealed that the soil was silty sand (SM) with low permeability. Tests on the mineral composition and microstructure fabric nature of the soil revealed that the soil was formed due to the weathering action of the parent charnockite rock. The finite element analysis of the slope was carried out using PLAXIS 3D. The analysis was carried out in two stages. The original slope before the vertical cut was modelled as the first stage. The vertical cut was modelled in the second stage to study the actual site condition before failure. The failure occurs due to the increase in pore water pressure in the soil, thereby reducing the matric suction and shear strength of the soil. The vulnerability of the building located near the cut slope is studied using the Support Vector Method to investigate the effect of material on the failure. The results showed the importance of the material properties in the increase of building resistance to 20%.

1. Introduction

Rainfall-induced landslide is a major threat to mountainous slopes all around the globe. The uprising frequency of development in landslide-prone areas increases the risk of landslides [1, 2]. India is among the top ten countries with the highest percentage of landslide fatalities for the years 2003, 2007, and 2008 [3, 4]. When rainfall exceeds the nominal rainfall in the monsoon season, the risk for landslides also increases [5]. The main factors for the initiation of landslides are antecedent rainfall and infiltration, as described by [6]. The leading cause of the rainfall-induced landslide is the increase in pore pressure and the reduction in mean effective stress in the slopes [7–13]. Two mechanisms are observed in rainfall-induced landslides [14]. First is the development of positive pore pressures in the soil-bedrock interface and hence the soil in the interface fails [15]. The second mechanism is due to the wetting of the soil in the slope, which causes the reduction in matric suction resulting in shallow landslides [16, 17].

Kerala is the third densely populated state in peninsular India. Nearly 47% of its land area is surrounded by the Western Ghats [18]. Kerala is divided into three distinct regions geographically: eastern highlands, central low lands, and coastal midlands. Precambrian and Pleistocene are the predominant geological formations covering most mountainous terrain with khondalite, gneisses, and charnockite rocks [19]. The landslides in the Western Ghats are mainly due to the climatic condition and the depth of the loose unconsolidated soil due to weathering. The soil stratum

consists of unconsolidated colluviums, lateritic soils, and lithomargic clay over Charnockite and Gneisses [19].

Very heavy rainfall in 2018 Southwest monsoon resulted in floods and landslides across Kerala. According to the Geological Survey of India (GSI), more than 67 major landslides and hundreds of minor landslides are reported. Among the 14 districts in the state, 13 of them were affected due to landslides of various types, scales, and dimensions [20]. More than 400 people died due to floods and landslides [21]. Average rainfall of 771 mm was recorded from the period of 1st to 20th August, and it is 140% more than the normal amount of rainfall [22], which caused many landslides and debris flow resulting in fatalities and heavy loss to infrastructure.

Nemmara landslide in Palakkad district, Peringavu and Kaithakunda landslides in Malappuram district, Karinchola landslide in Kozhikode district, and Upputhode landslide in Idukki district are some of the significant landslides that occurred during the 2018 southwest monsoon. The present study discusses the detailed investigation of the Kaithakunda slide by geotechnical characterization of the soil slope and the influence of weathering in the slope and slope stability analysis using a 3D finite element model.

The physical vulnerability of the building to slope failure is essential for the risk definition [23]. It is the degree of loss of an element or a given set of elements in a hazard area [24]. For assessing the structural loss, the vulnerability of the building at risk is obtained by analyzing the damage degree from the type and intensity of landslide [25]. Studies were carried out to find the vulnerability using vulnerability curves and matrices, but they neglected the building properties that led to the vulnerability [26]. There are studies related to finding the residual lateral thrust on the footing sides of the wall through nominal codal provisions but no deterministic studies to find the parameters required for the probabilistic analysis are carried out till now [26, 27]. There are very few studies related to the vulnerability of buildings in the cut slope, and hence a detailed study of the vulnerability of the buildings is needed. This study helps in vulnerability assessment in terms of mechanics and its effect on vertical cut slope failure. The method used will be helpful to planners and engineers on the variables that make the structure vulnerable during cut slope failures.

2. Building Failure in Kaithakunda

The slope failure occurred at Kaithakunda (11°10′ 59.59″N, 75°53′ 48.37″E) located in Malappuram district, Kerala state of India (Figure 1). The slide occurred at 1 AM on August 16, 2018, and damaged a house, as shown in Figures 2(a) and 2(b). It led to the death of 3 people [28]. The failure of the slope is observed as a vertical cut failure, as shown in Figures 2(c) and 2(d). Figures 2(e) and 2(f) show the mudslide into the house that led to the death of three people. The overall plan of the area and the longitudinal section of the slope are shown in Figures 3(a) and 3(b), respectively.

The building is a load-bearing structure and the material used for the construction is laterite block obtained from the local area. The building is a single-storey building with two columns to support the front porch of the building. Figure 2(b) shows the tilting of the column in the portico of the building and wide cracks in the building. As can be observed from Figure 3(b), the building was constructed after cutting the original slope vertically for about 11.5 m. No stabilization measure was adopted for the vertical cut. The building was located 3 m from the vertical cut. The vertical cut of the slope extended up to 20 m in width. At the top of the cut, another building applied the surcharge load on the vertical cut. The main reason for the occurrence of the slide is the heavy rainfall experienced in the area. The rainfall occurred in two stages, with the 1st stage of very light rainfall between June and July 2018. The second stage of rainfall occurred from August 1 to August 14. The third stage consists of very heavy rainfall during and August 15–16, 2018.

3. Rainfall Data

The rainfall in Kerala consists of two monsoons, namely, the Southwest monsoon and Northeast monsoon. The Southwest monsoon starts in early June and ends in August. The Northeast monsoon starts in October and ends in November [29]. The location of rain gauge stations in the Malappuram and Kozhikode districts is depicted in Figure 4(a). Two rain gauge stations are located near the site: one at Karipur Airport in Malappuram district and the other at Kozhikode in Kozhikode district. Rainfall data from the rain gauge station at Karipur airport is considered for further analysis due to its proximity to the site. Cumulative rainfall of Malappuram district during the Southwest monsoon 2018 is compared with the average cumulative rainfall data of the previous 50 years, as shown in Figure 4(b) [22]. Cumulative rainfall data for the event year (2018) is 2600 mm, 44% higher than 50 years average rainfall (1800 mm). Daily rainfall recorded at Karipur airport during August 2018 is depicted in Figure 4(c). The landslide occurred at 1 AM on August 16, 2018. As can be observed from Figure 4(c), the daily rainfall on the event day is 175 mm. The importance of antecedent rainfall in triggering the landslide can be observed as the heavy rainfall on the event day was preceded by heavy rainfall on the 14th and 15th of August 2018.

4. Tests on Soil Samples

The top layer of the soil extends up to a depth of 6 m from the ground surface. The second layer extends from 6 m to the bedrock. The top layer is highly weathered in nature and reddish compared to the second layer of soil, which is white. The slip surface is found in both the top and second layers of the soil, as can be seen from Figure 2(d). The geological map of the Malappuram district, as developed by the Geological Survey of India [30], is depicted in Figure 5. The figure indicates the occurrence of charnockite rock in the study area [31]. The geology and geomorphology of the site location indicate that the soil is formed due to the weathering action of the parent charnockite rock.

The soil samples were collected from the slip plane: one at 1.5 m depth in the topsoil and the other at 6.5 m depth in

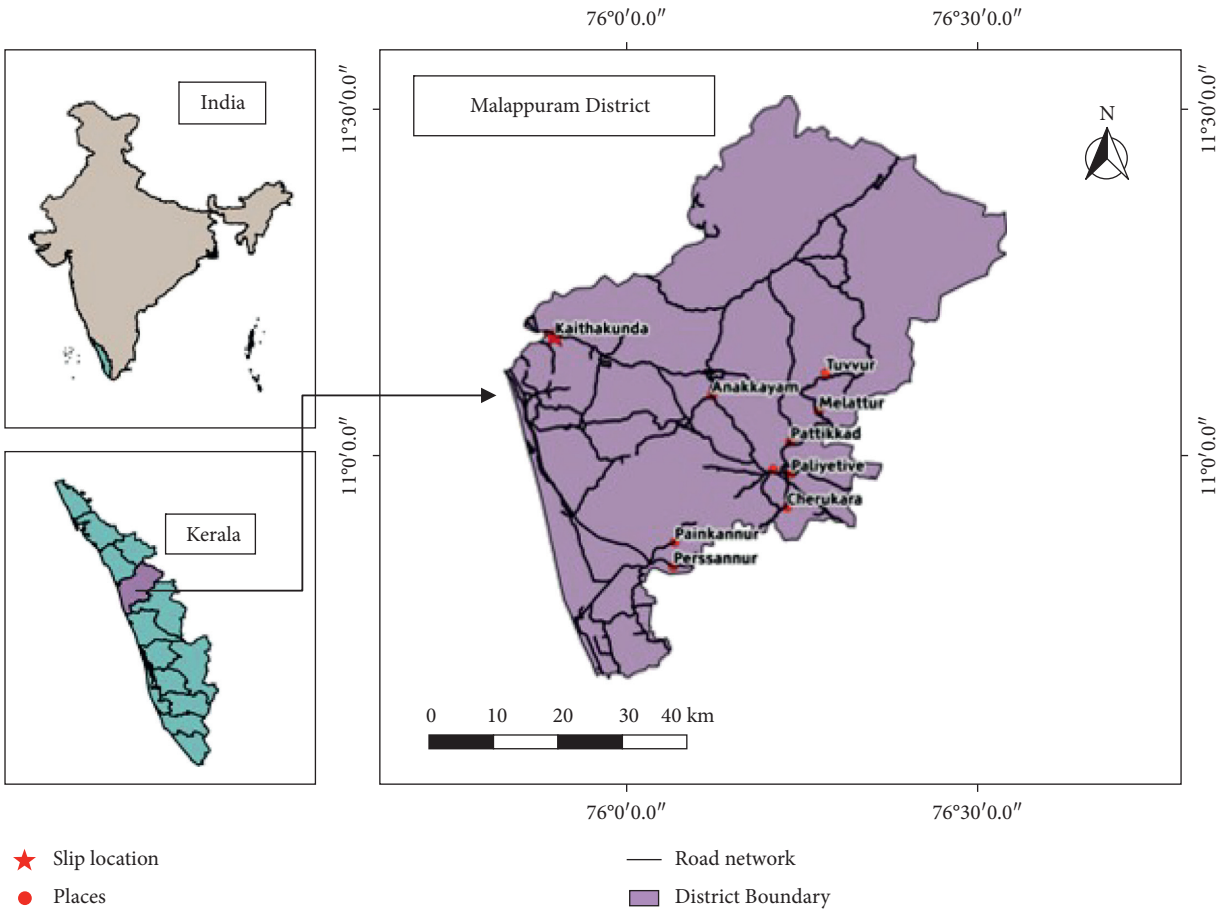

Figure 1: Geographical location of slope failure at Kaithakunda, Malappuram district, Kerala, India.

the second layer (Figure 2(d)). The characteristics of the soil layer are found through laboratory tests. Index and engineering properties of the soil samples are evaluated by carrying out laboratory tests as per ASTM standards. Sedimentation analysis was carried out to identify the amount of clay and silt content.

The mineral composition and the microfabric nature of the soil were identified by X-ray Diffraction (XRD), Field Emission Scanning Electron Microscopy (FE-SEM), and Energy-Dispersive X-ray spectrum (EDX).

5. Analysis Using the Finite Element Method

The finite element analysis is carried out using PLAXIS 3D. The analysis is carried out in three phases.

5.1. Analysis of the Original Slope. To understand the behaviour of the natural slope, the analysis is carried out on a model of the original slope. Figure 6 shows the model of the original slope with two layers of soil and one layer of rock. Slope with dimensions of 104 m length, 30 m width, and 33 m height is considered in the analysis. The properties of soil and rock are presented in Table 1. The soil is modelled as 10-node tetrahedral elements. The soil is modelled as Mohr–Coulomb elastic perfectly plastic model [32]. The hydraulic boundary condition (X, Y), Z_{min} are considered as open for the analysis and all other directions with respect to Z are closed. The undrained shear strength of the soil is modelled using effective stress analysis with the effective shear strength parameters. Fully coupled flow deformation analysis is carried out to study the coupled effect of flow and deformation in the unsaturated soil due to the change in hydraulic boundary conditions with respect to time [33]. The initial stage of the calculation is carried out with gravity loading for the attainment of the geostatic equilibrium of the slope [34].

5.2. Infiltration Analysis. For the infiltration analysis, the soil condition is taken as unsaturated and Soil Water Characteristic Curve (SWCC) is considered to describe the hydraulic parameters of the groundwater flow in the unsaturated soil. The infiltration analysis is carried out by the van Genuchten method [35]. S_e is the effective saturation and is given by

$$S_e = \frac{S - S_{res}}{S_{sat} - S_{res}}.\text{and,}$$
$$S_e = \left[\frac{1}{1 + (\varphi/\alpha)^n}\right]^l. \quad (1)$$

FIGURE 2: View of building failure. (a) View of the damaged house with vertical cut. (b) Elevation of damaged building. (c) Sliding part of the failed cut. (d) View of vertical cut failure. (e) Detailed view of the damaged portion. (f) Outside view of the damaged portion.

And S_{res} is the residual saturation in the soil and S_{sat} is the full saturation level in the soil. Soil saturation is a decreasing function of the matrix potential. van Genuchten (1980) provides the relation between effective saturation and matric suction potential, where φ is the matric suction potential and α, n, and l are the curve fitting parameters. This

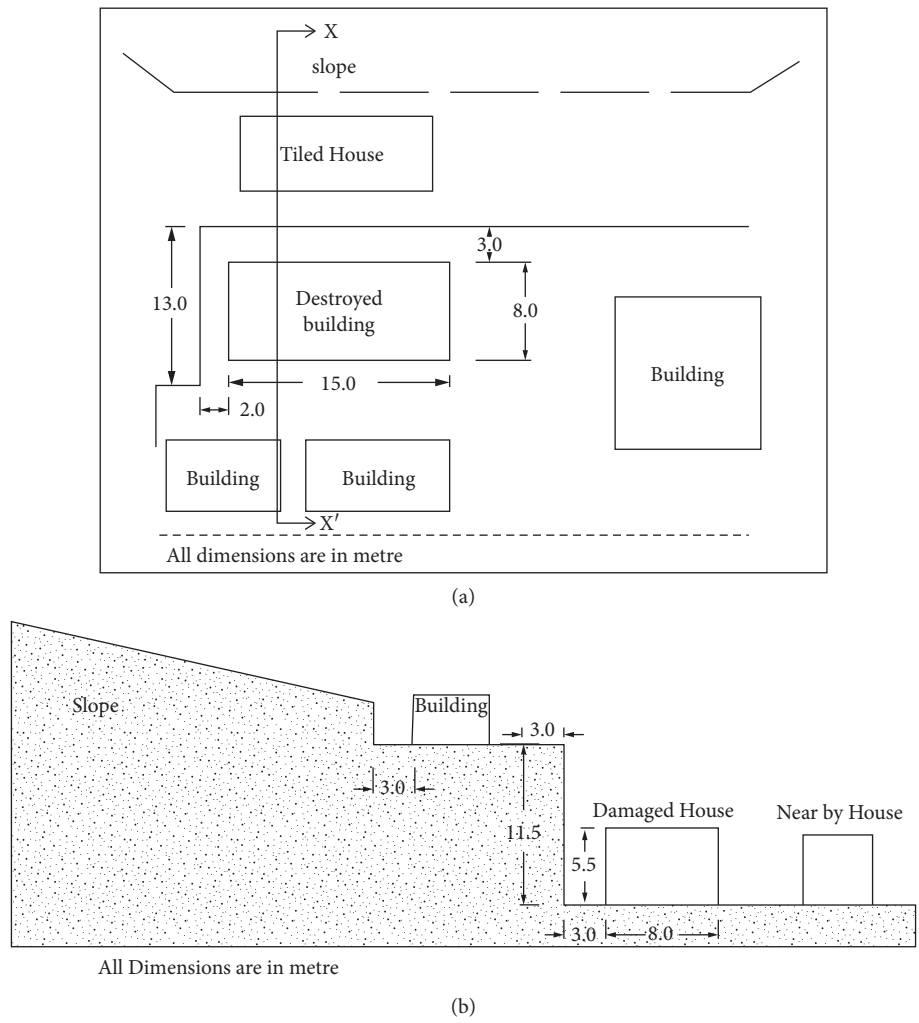

Figure 3: Geometry of the slope with vertical cut and buildings: (a) plane and (b) longitudinal section.

can be found out by Soil Water Characteristic Curve (van Genuchten, 1980). Based on the suggestion of [36], the typical capillary curve for silty material and sand was obtained from [37]. The van Genuchten parameters for sandy silt and sand were obtained from the unsaturated soil hydraulic database (UNSODA) [38, 39]. The van Genuchten fitting parameters (α, n, l) of the topsoil and bottom soil are 0.010, 0.45, 0.089 and 0.029, 0.47, 0.069, respectively.

5.3. Analysis of Vertical Cut. Finite element analysis of the site condition that existed before failure (Figure 3(b)) is carried out to evaluate the mechanism of failure. Figure 7 shows the geometry of the model before slope failure. It shows the vertical cut in the slope and the building located very close to it. The structure is a single-storey building with load-bearing walls. The building is modelled as a plate element. Beam elements are used to transfer the load from the roof to the plates (load-bearing walls) (Figure 7). The foundation of the building is considered as a plate element to transfer the load to the soil. The plate and beam elements are modelled with a unit weight of Reinforced Cement Concrete (RCC). The width and length of the building are taken as 8 m and 15 m, respectively (Figures 8, 2(a), and 3(a)). The beam and plate elements are considered with a minimum thickness of 125 mm and 75 mm, respectively. The effect of a tiled roof building located above the vertical cut (Figure 3(b)) is considered as a surcharge load (20 kN/m^2) in the analysis.

The modelling and properties of soil and the method of analysis were already discussed in the previous section. Infiltration analysis was carried out to study the effect of slope on the building. The rainfall data were used for infiltration in surface groundwater flow boundary conditions. The rainfall data obtained from the Indian Meteorological Department (IMD) are shown in Figures 4(b) and 4(c). The analysis was carried out in three stages. The first stage considered continuous rainfall of low intensity (cumulative rainfall of 1770 mm) from June to July 2018. The second stage considered intense rainfall from the 1st of August to the 14th of August 2018. The rainfall recorded during the second stage (August 1–14) is 2800 mm. Since the failure of the slope was observed on August 16, the third stage of analysis was carried out by considering the rainfall that occurred on the 15th and 16th of August with a very high intensity of 187.5 mm/day (Figure 4(b)).

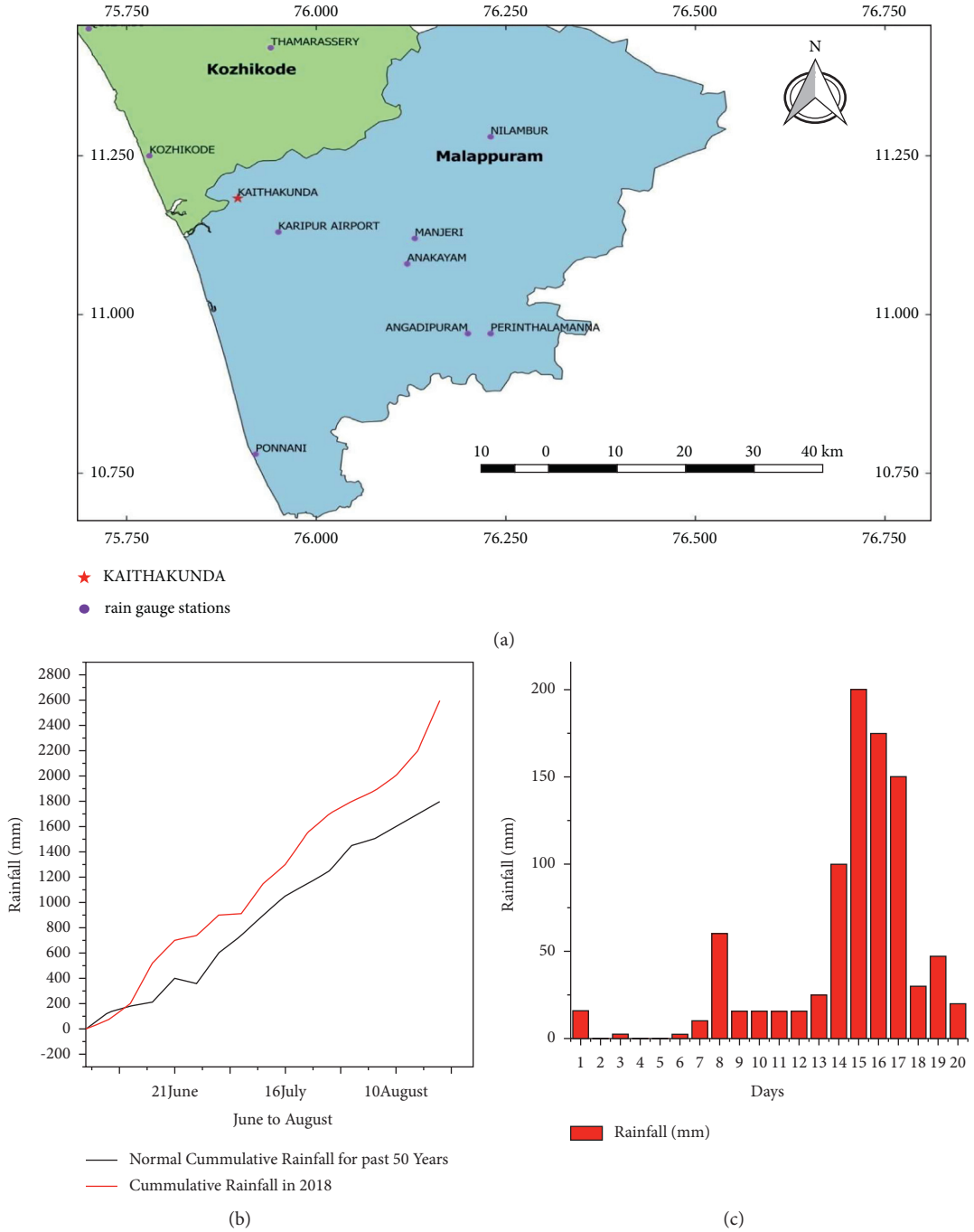

Figure 4: Rainfall data. (a) Rain gauge stations near Kaithakunda. (b) Cumulative rainfall for south-west monsoon 2018 (after IMD 2018). (c) Daily rainfall recorded at Karipur airport in August 2018 (after IMD 2018).

6. Vulnerability of the Building Located near the Vertical Cut

To evaluate the vulnerability of buildings during vertical cut failure, the forces acting on the building are required to be calculated. Factors such as geological and structural features of buildings play a vital role in physical vulnerability. The vulnerability based on indicators is used to define the vulnerability of the building. The process used in this analysis is the calculation of the residual thrust force of the slope failure through Finite Element Analysis (FEA). In FEA, the residual force acting on the sides of the building is calculated by considering the interface elements between the soil and the structure [40]. The building thrust force, height, length, width, and material properties of the building are used as indicators to find the vulnerability of the building for this particular type of soil surroundings [41–44]. The indicators are selected based on the available characteristics and the results from the deterministic model.

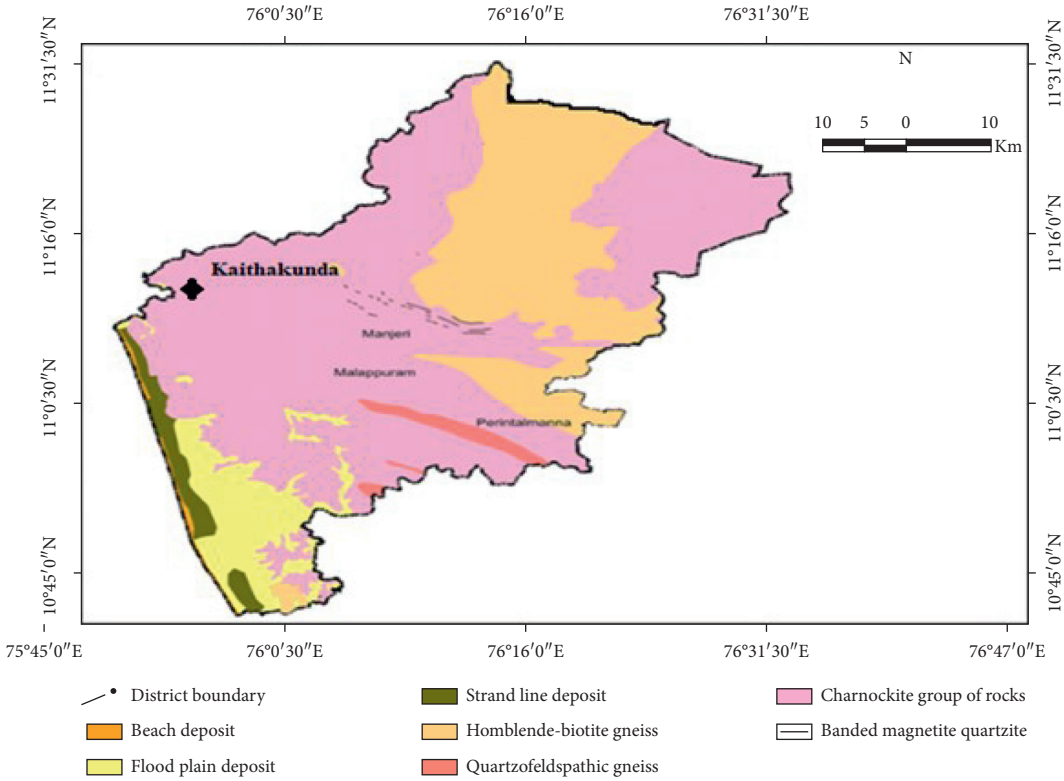

Figure 5: Geological map of Malappuram district (after GSI 2005).

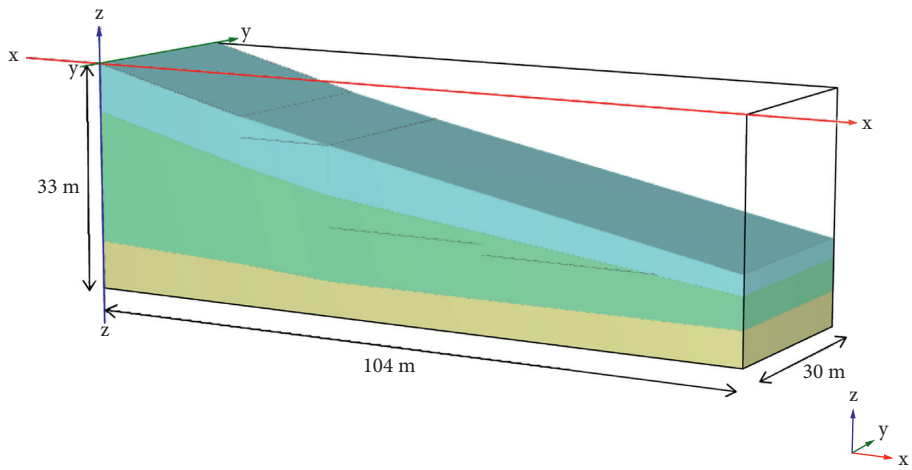

Figure 6: Finite element representation of the original slope geometry.

Table 1: Properties of soil and rock.

Property	Layer 1—soil	Layer 2—soil	Layer 3—rock
Specific gravity (G)	2.48	2.57	—
Liquid limit (w_1) (%)	49	49	—
Plastic limit (w_p) (%)	34	29	—
Plasticity index (I_p) (%)	15	20	—
Soil classification	SM	SM	Soft rock
Coefficient of permeability (k) (m/s)	5.54×10^{-8}	1.88×10^{-7}	—
Effective cohesion (c') (kN/m^2)	10.90	9.86	0
Effective friction angle (φ') (°)	20.06	22.10	55
Elastic modulus (E) (kN/m^2)	14×10^3	16×10^3	70×10^3
Poisson's ratio (ν)	0.325	0.325	0.35
Dry unit weight (γ) (kN/m^3)	18.55	19.90	26
Dilatancy angle (ψ) (°)	0	0	0

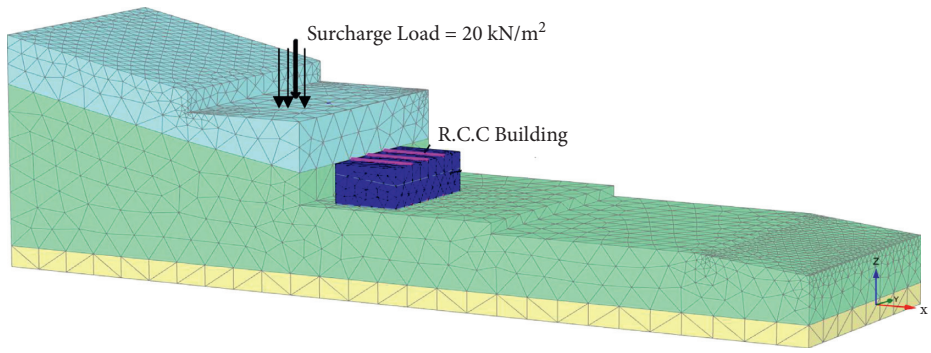

Figure 7: The geometry of the model existing site condition before failure.

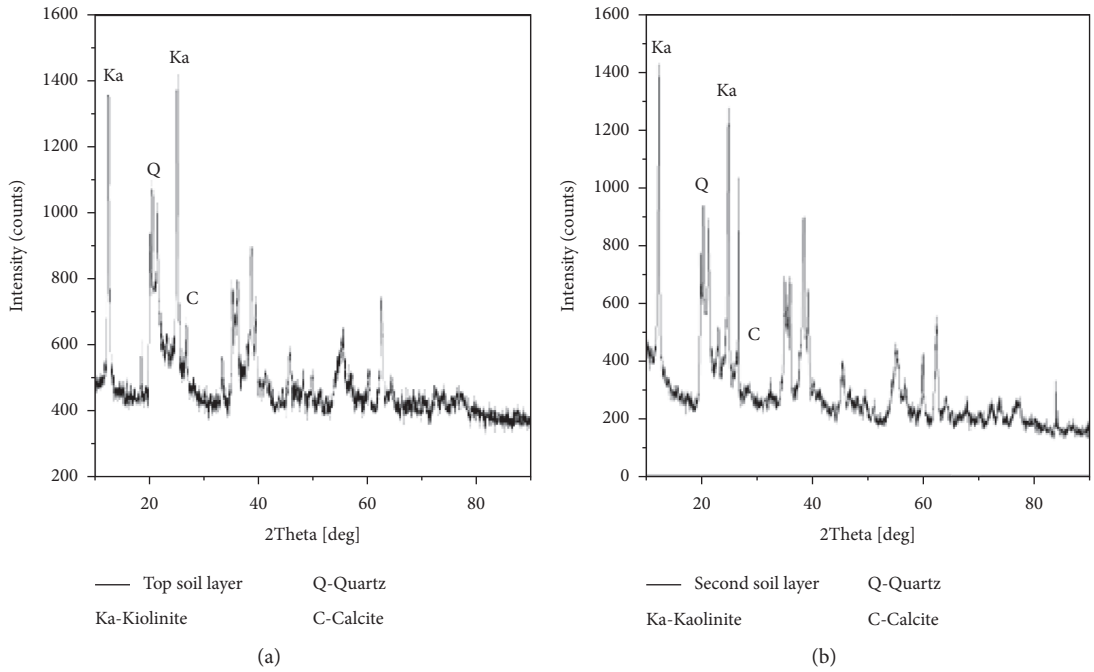

Figure 8: X-ray diffraction pattern for (a) the topsoil layer and (b) the bottom soil layer.

The undrained soil parameters are given as input for the deterministic analysis in the numerical model. The groundwater infiltration was carried out using the rainfall data for June–August 2018. The vulnerability of the building based on the inclination of the building is used in the study. Thus, when the vulnerability value reaches 1, then the building is subjected to failure and when the vulnerability is less than 0.2, it is safe [26, 27].

Vulnerability based on the inclination of the building is used to define the degree of damage to the building [45]. The inclination is calculated with respect to the deflection of the building. Analytically, the Timoshenko function of deflection for a uniform loaded beam is used to find the deflection [27, 46].

$$y_m = \frac{5qL^4}{384EI} + \frac{3qL^2}{16GA}, \tag{2}$$

where y_m is the maximum deflection of the beam, q is the lateral thrust of the structure, and L and W are the length and width of the structure. E and G denote the elastic and shear modulus of the building material.

6.1. Inclination and Lateral Thrust Calculation. The inclination of the building is the ratio of horizontal deflection to the vertical height of the wall. The inclination of the building is defined as

$$i = \frac{y_m}{H}, \tag{3}$$

where i is the inclination of the building, y_m is the horizontal deflection of the building, and H is the vertical height of the building. According to [47], the allowable deflection is 1.6 cm, and this is classified as safe.

The lateral thrust is calculated from the finite element model by considering the interface between the structure and the soil. Interfaces are used to study the interaction between the structure and soil [33, 47]. The interface describes the friction between the structure and the soil, which is usually 2/3 of the soil friction angle. The interface element helps to obtain the effective horizontal stress acting on the structure, which are the lateral Earth pressures acting on the structure [33].

6.2. Damage Degree of Inclination. The ratio of the inclination of the building to the threshold value (i_m) is defined as the damage degree, which is the physical vulnerability (v) [48, 49]. The degree of damage can be evaluated by parameters such as cracks, inclination, and maintenance cost [50, 51]. The vulnerability in the vertical cut slope failure is developed with the inclination, which is defined as the function of building lateral thrust, building material properties, dimension of the building, and the height of the building. Vulnerability of building is given by [27]

$$v = \begin{cases} \dfrac{i}{i_m} = \dfrac{1\left(5qL^4/384EI + 3qL^2/16GA\right)}{Hi_m}, & \begin{pmatrix} i < i_m \\ i \geq i_m \end{pmatrix} \\ 1, \end{cases} \quad (4)$$

where i_m is the permissible inclination of the building. According to Kotlicki and Wysokinski, the permissible value of deflection is 25 mm for the masonry building with reinforced concrete slabs and beams, and the i_m value is limited to 0.008.

The vulnerability (v) is from 0 to 1, where 1 indicates severe damage and 0 indicates being safe. The deformation of the building is calculated with the help of unsaturated soil parameters and hence the soil deformation is studied to give real-time vulnerability of the building.

6.3. Vulnerability Using the Support Vector Method. The optimization or calibration of the parameters used for the vulnerability analysis is analyzed through the Support Vector Method (SVM) in machine learning. Khalil et al. compared different machine learning techniques for approximating groundwater models, which are complex whereas SVM was found to reduce the error in the fitting of the indicators. SVM solves both optimization and regression problems. Many of the SVM applications have predicted very good results [52–56].

In this study, SVM is used to predict the vulnerability of buildings in the vertical cut slope failure. For the regression problem, two subsets are used, and they are as follows: (1) training subsets to construct the model and (2) a testing subset to estimate the model performance [57]. The training, testing, and normalization techniques are used for the prediction. The input parameters are q (lateral thrust of the structure), H (height of the structure), E (elastic modulus of the building material), L and W (length and width of the structure), and v (vulnerability) is the output of the model. RStudio platform is used for conducting the regression analysis in this study.

7. Results and Discussion

7.1. Properties of Soil. The particle size distribution curve for the soil samples is shown in Figure 9. Properties of soil evaluated from lab tests are presented in Table 1. Both soils are identified as silty sand (SM) as per USCS classification [58]. Hydraulic conductivity of the soil sample is evaluated as per the Indian Standard Code [59] and the permeability values for both the soil samples are in the range of 10^{-7} to 10^{-8} m/s. The Proctor compaction test is carried out to determine the maximum dry density of the soil. Consolidated drained (CD) direct shear tests on the soil samples are conducted as per [60]. The effective shear strength parameters obtained from the tests are presented in Table 1.

7.1.1. Weathering Characteristics. Figure 10 depicts FE-SEM images of both layers of soil. Figure 10(a) indicates that the topsoil layer was governed by silt/clay size clusters with voids on the soil particle surface and a highly porous structure due to the high weathering. The degree of weathering reduces with the increase in depth as the presence of clay minerals and pore volume decreases (Figure 10(b)). The FE-SEM images of both soil layers show the presence of kaolinite clay mineral with many pores in it, which is well supported by EDX and XRD analysis, as shown in Figures 8 and 11. EDX and XRD results indicate the presence of kaolinite clay mineral ($Al_2Si_2O_5(OH)_4$) along with quartz and calcium carbonate ($CaCO_3$) in the topsoil (Figures 8(a) and 10(a)) [61, 62]. The presence of calcium carbonate in the soil indicates the weathering process in the soil [62, 63]. The second layer of soil has a very less amount of kaolinite clay due to the incomplete weathering process (weathering degree-VI according to [64]) in the soil [63, 65] (Figures 8(b) and 11(b)).

Charnockite rocks are the parent rocks present in the Malappuram district and the weathering action of the rocks results in laterite soil, which is reddish brown [66]. The second layer of the sample is white due to the formation of calcium carbonate ($CaCO_3$) in the soil (Figure 2(d)). Charnockite is a felsic rock present in the lower crust containing minerals, such as orthopyroxene and garnet [67]. The property of the bedrock is shown in Table 1. Most of the laterite soil in the region covers up to 25mm depth and is underlain by charnockite rocks [68]. Due to the granulite facies metamorphic event, the felsic magmas are hydrated to form the charnockite rock [67].

7.2. Results of Finite Element Analysis

7.2.1. Original Slope. Rainfall data from June to August 2018 (Figure 4(b)) were considered for the infiltration analysis. The rainfall with low intensity and high intensity were carried out in separate stages (the cumulative rainfall of the first stage (June to July 2018) is 1770 mm and the second stage (August 1–14) is 2800 mm). At the end of the first

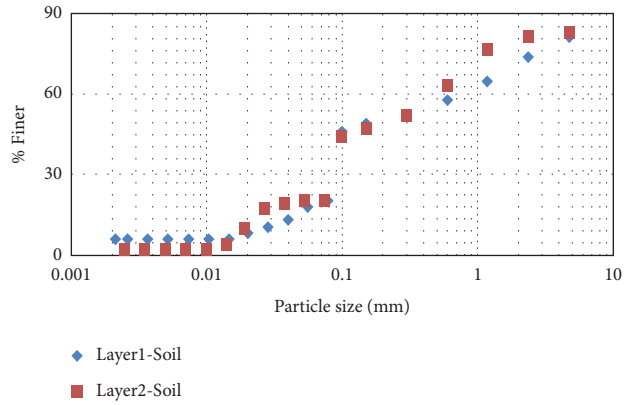

Figure 9: Particle size distribution curve.

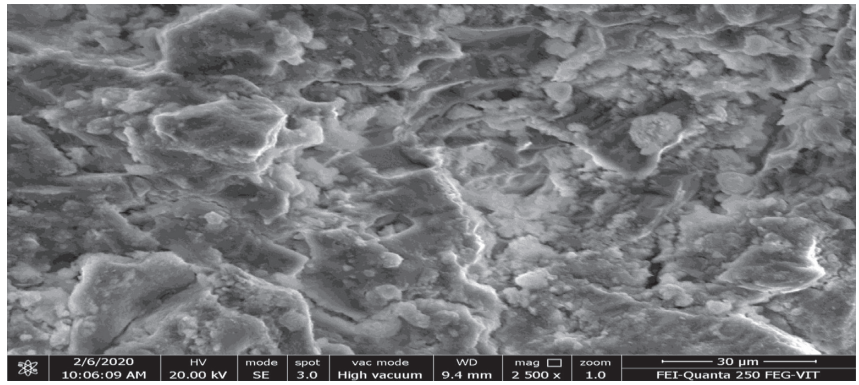

(a)

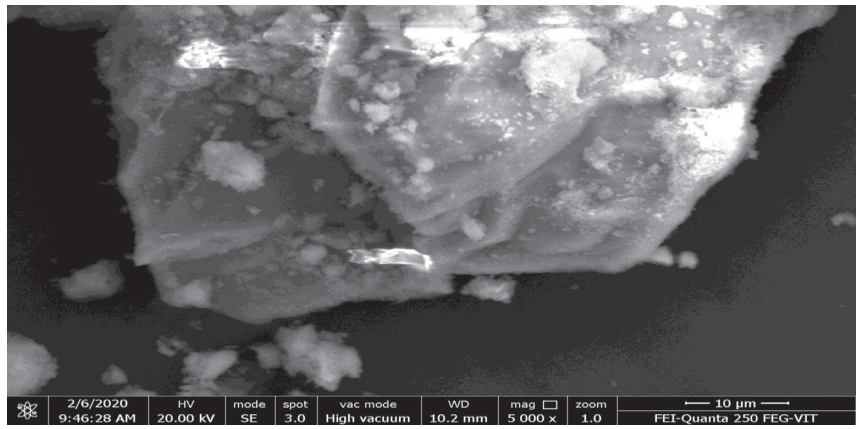

(b)

Figure 10: FE-SEM images of (a) topsoil and (b) second-layer soil.

stage, there was no significant displacement. The pore water pressure and the displacement of the original slope at the end of the second stage are shown in Figures 12(a) and 12(b), respectively. The pore pressure, as observed in Figure 12(a), indicates that the matric suction of the soil is more and hence negligible displacement in the slope, as shown in Figure 12(b) [69]. This indicates the stability of the original slope.

7.2.2. Results of Vertical Cut Analysis. The details of the beam and plate elements are given in Table 2. The deformed mesh is shown in Figure 13(a). The deformed mesh indicates the caving of the vertical cut. The shape of the deformed mesh indicates the failure of the vertical cut. The displacement profile of the slope (Figure 13(b)) indicates that the maximum displacement occurred at the top of the vertical cut. It depicts the slip surface of failure as observed

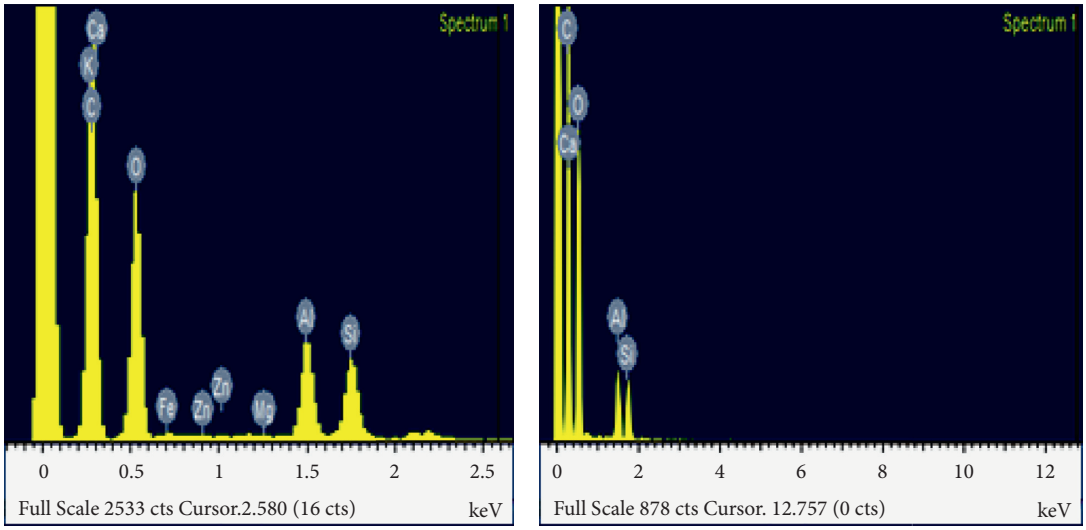

(a) (b)

Figure 11: Energy-dispersive X-ray spectrum. (a) The topsoil layer and (b) the bottom soil layer.

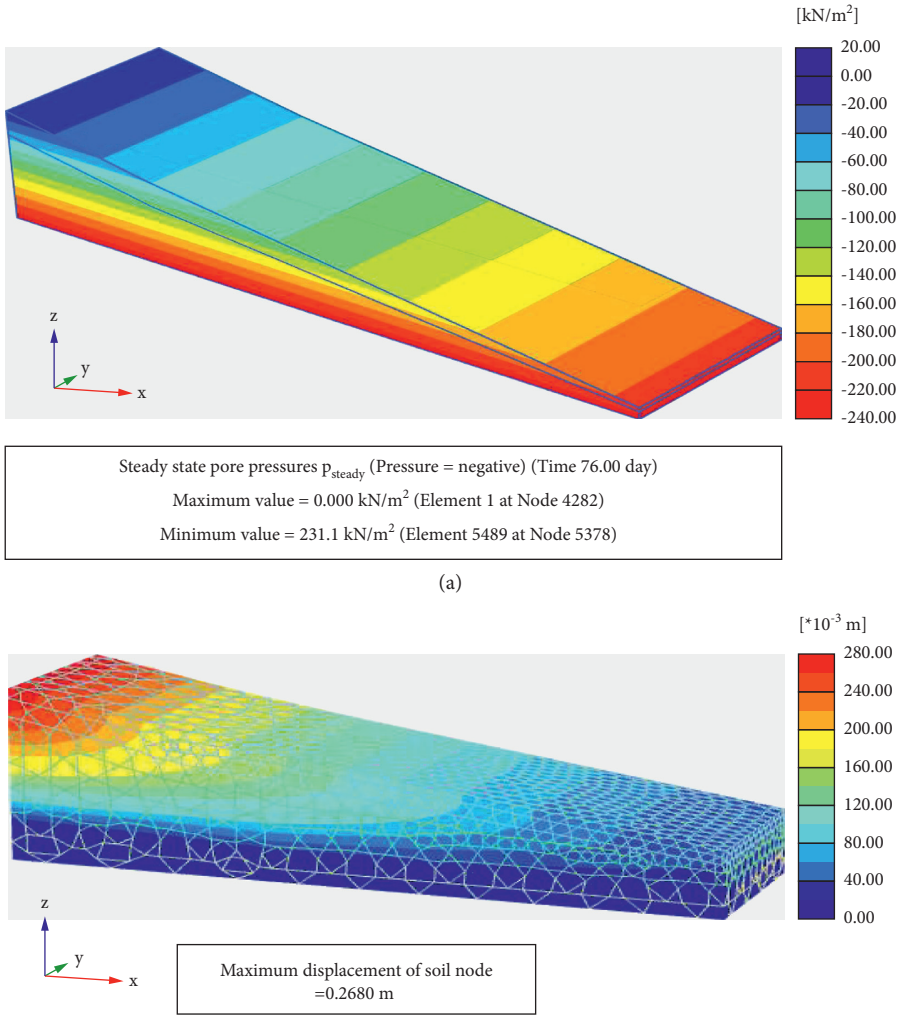

Figure 12: Finite element representation of the original slope. (a) Pore water pressure development. (b) Displacement contour.

Table 2: Building properties.

Property	Building	
	Plates	Beam
Density (kN/m^3) (γ)	25	25
Elastic modulus (kN/m^2) (E)	30×10^6	30×10^6
Poisson's ratio (ν)	0.2	0.2

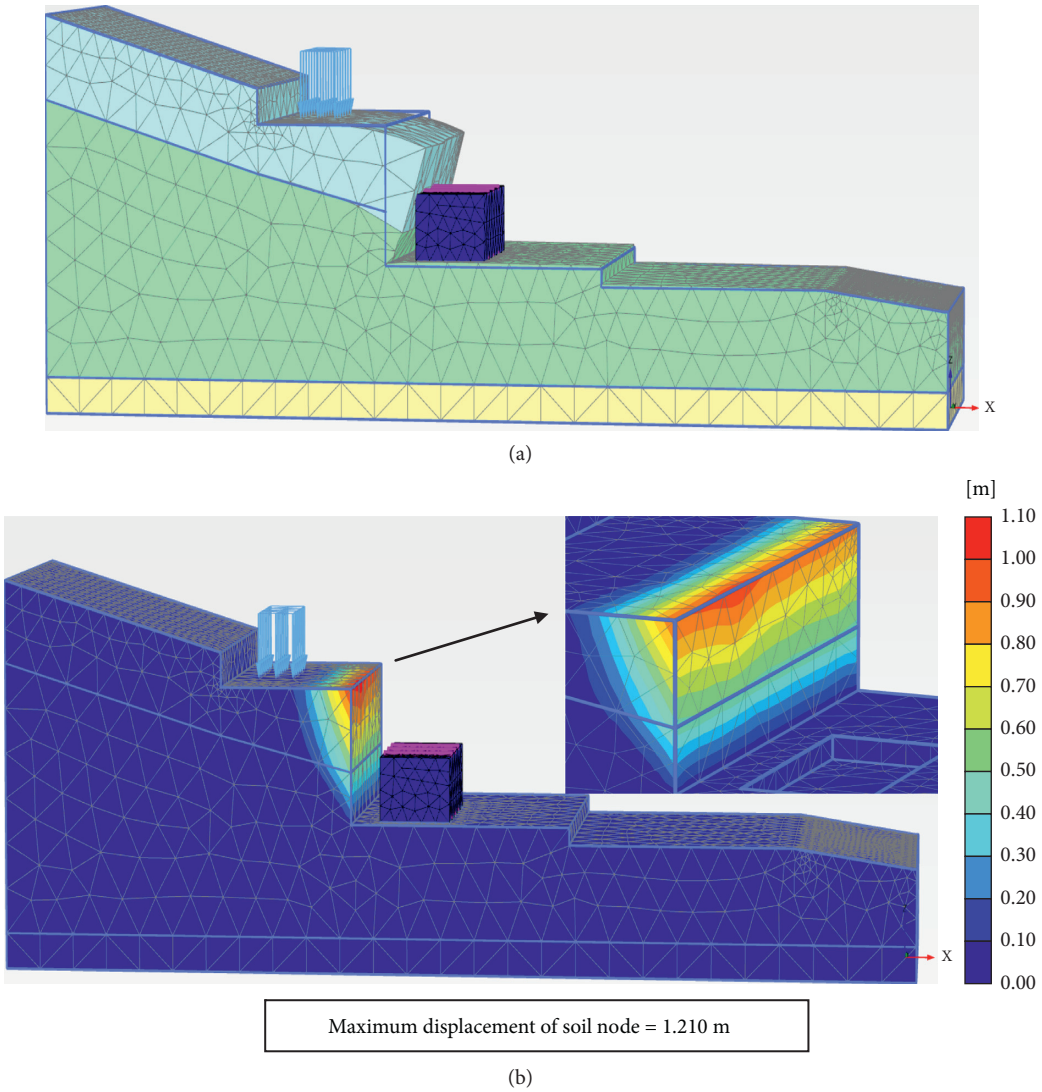

Figure 13: View of vertical cut failure. (a) Deformed mesh. (b) Displacement profile for vertical cut.

from the field (Figure 2(c)) and indicates the displacement of the soil node as 1.20 m.

Figure 14(a) shows the maximum displaced nodal position of the model. The calculation is carried out with infiltration analysis and the maximum value of the displaced soil node is found to be 1.210 m at the position of the node (40, 9.737, −8.9), as shown in Figure 14(a). The figure shows that the maximum displacement of the soil from its original position before deformation is 4.1 m. The rotation of the soil node is found to be 4.667 degrees. As the distance between the vertical cut and the building is 3 m (Figure 3(b)), the displacement of soil, flow pattern, and plastic points of soil observed from Figures 13(a), 13(b) and 14(a) and 14(b), the sliding soil reaches the building, which caused tilting and severe damage of the building (Figures 2(e) and 2(f)) and hence the building wall is deformed to a distance of 45 cm from its original position, which is visible from Figure 2(d). Figure 14(b) shows the plastic points of the model slope with the failure points occurring at the toe of the cut and it progresses to the topsoil layer. The tension cut-off point refers to the movement of the soil due to the failure. The red cube indicates the development of failure stress in the failure

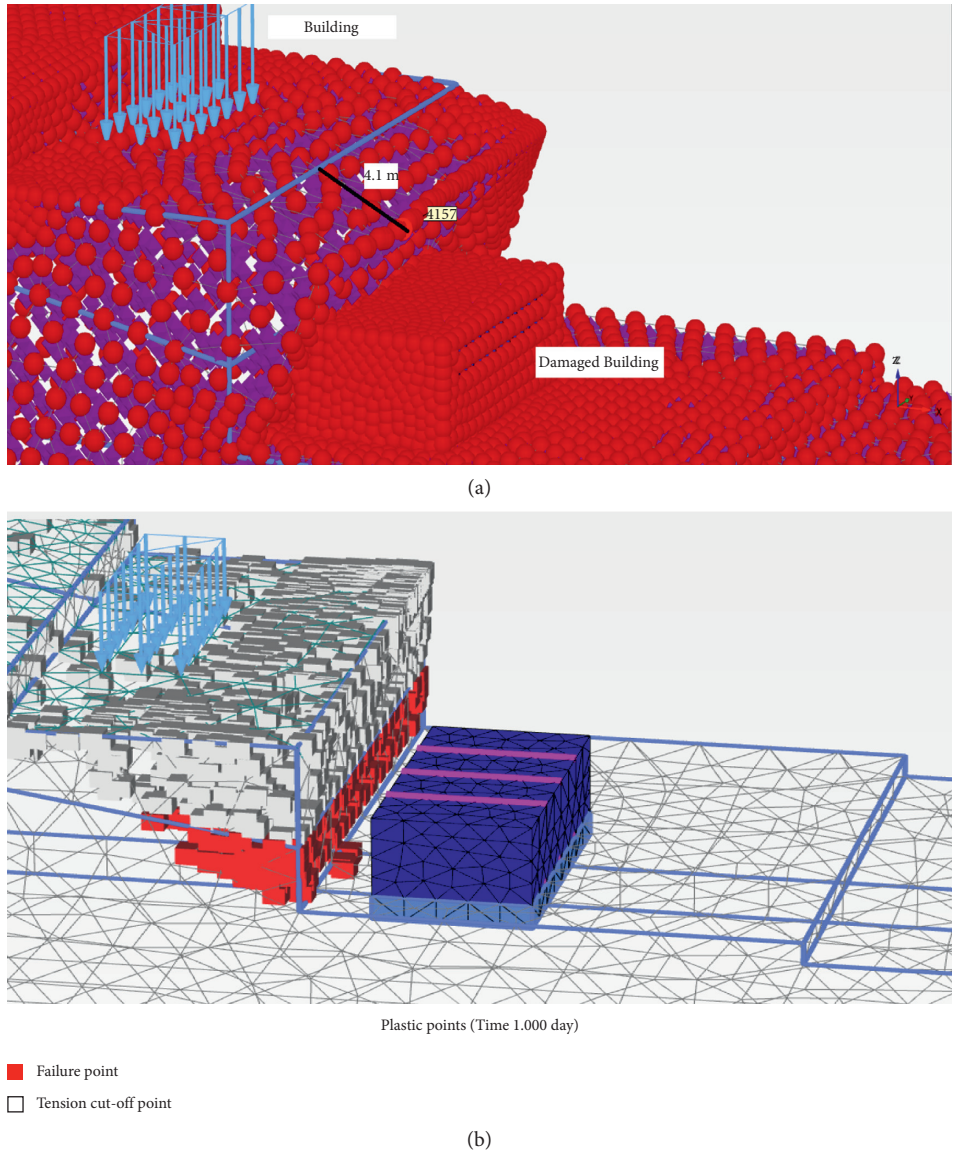

Figure 14: Detailed view of (a) maximum displaced node (node no. 4157) and (b) plastic points in the model.

envelope and the tension point is a point that fails in tension [33]. The results indicate that the soil displacement at the top of the vertical cut is more. As can be observed from Figures 3(b), 13(a), 14(a), and 15(a), the saturation level of soil cross section close to the vertical cut at $X = 39.55$ m and $Z = -8.9$ m indicates that the soil at the top level is saturated more. It can be observed from the figure that the saturation level of soil reaches up to 100% of the soil located at the top of the vertical cut. The saturation contour at a level of −20.90 m indicates the saturation level of nearly 65% and this leads to the increase in pore water pressure and a decrease in the effective stress as shown in Figure 15(b).

The effective stress for the soil at various stages of rainfall indicates the reduction in stresses due to the increase in pore pressure, and it can be visible that the effective stresses decrease and reach constant value for all three stages (Figures 15(b) and 15(c)) [12]. The pore water pressure for different stages of rainfall is depicted in Figure 15(d). The first stage of rainfall indicates the suction pressure is more due to the unsaturated state of soil and hence the slope is stable. This is due to the increased shear strength of the soil. The second stage (August 1–14) and the third stage (August 15–16) denote the fact that the pore water pressure increases at the top of the soil due to the increase in saturation level (Figure 15(a)). The increase in the pore water pressure at the third stage results in the reduction of effective stress (Figure 15(b)) and thereby, it reduces the shear strength of the soil at the vertical cut. This leads to the failure of the slope, as shown in Figures 13(a) and 13(b). The values from the numerical analysis were validated against the analytical values (Bishop's effective stress) used in the PLAXIS 3D software to emphasize the importance of the reduction in the effective stress at the end of the third stage. Figure 15(c) shows a slight variation from the numerical analysis in the analytical formula and this is due to the assumption that

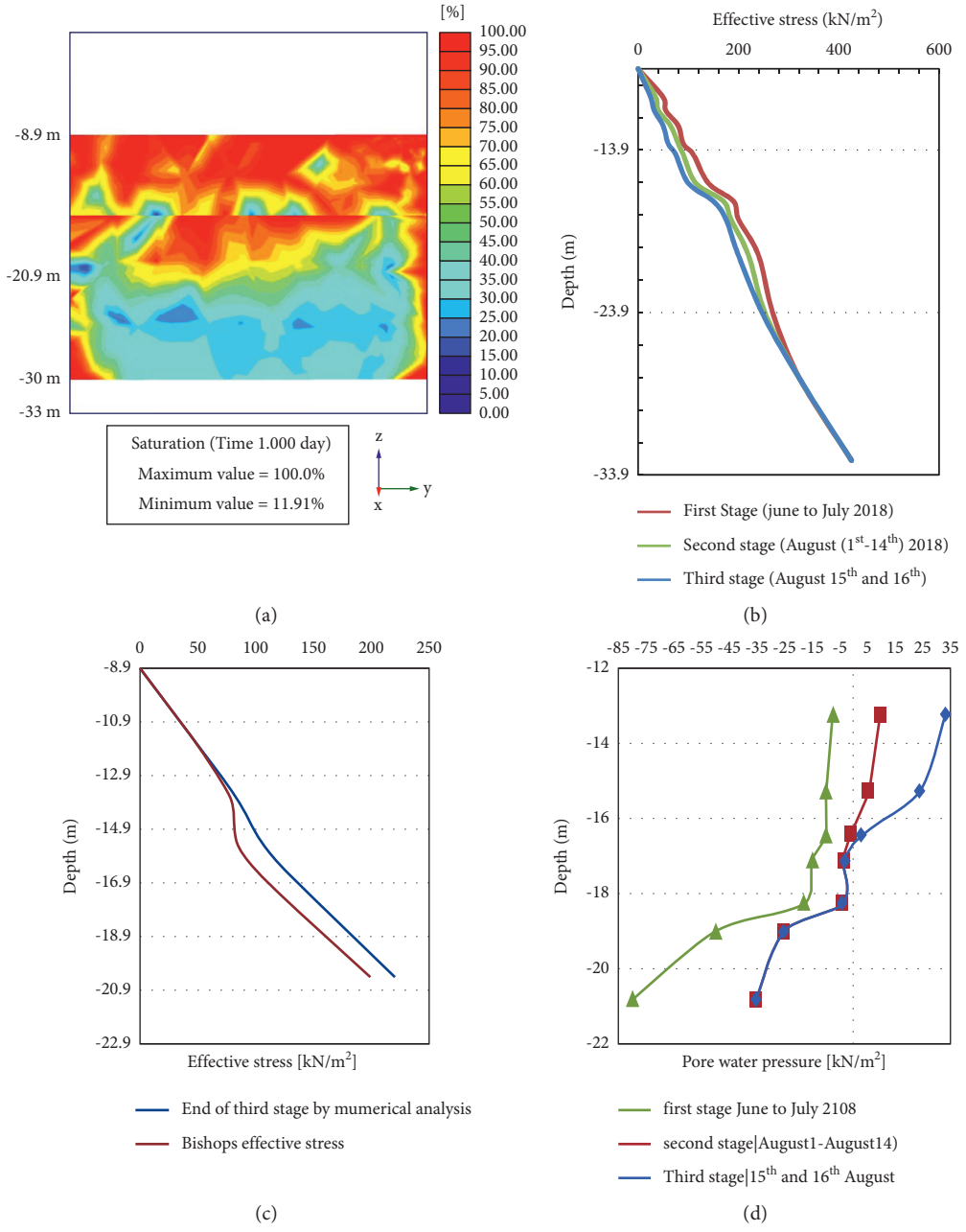

Figure 15: Results of numerical analysis. (a) Saturation level of the soil cross section at $x = 39.55$ m and $Z = 8.9$ m at vertical cut. (b) Effective stress at various stages. (c) Effective stress validated with the analytical method from PLAXIS 3D. (d) Pore water pressure of the soil at various stages.

pore air pressure used in PLAXIS is zero at the reference level [33].

The slope is stable at the end of the first stage of rainfall (Figure 15(d)) and this is due to the increase in matric suction in the soil. This is well supported by the increase in the effective strength of soil (Figure 15(b)). During the second stage of rainfall, the slope gets saturated and thereby, the pore water pressure increases. The increase in pore water pressure causes the effective stress to be reduced. The third stage causes the slope to be saturated (saturation up to 80%) for a depth of 8 m from the ground surface of the vertical cut. This causes the soil to develop an intense increase in pore water pressure (Figure 15(d)) of 35 kN/m^2, which is accompanied by a decrease in effective stress of 25 kN/m^2. This reduction in the effective stress of the slope results in its failure (Figure 13(a)). The displacement of the soil is found to be 4.1 m from the top of the vertical cut (Figures 14(a) and 14(b)) and hence the displaced soil from the vertical cut caused the building to fail as observed from Figures 2(e) and 2(f).

7.3. Results of Vulnerability Analysis. The model used for the analysis uses the polynomial kernel, which has an R^2

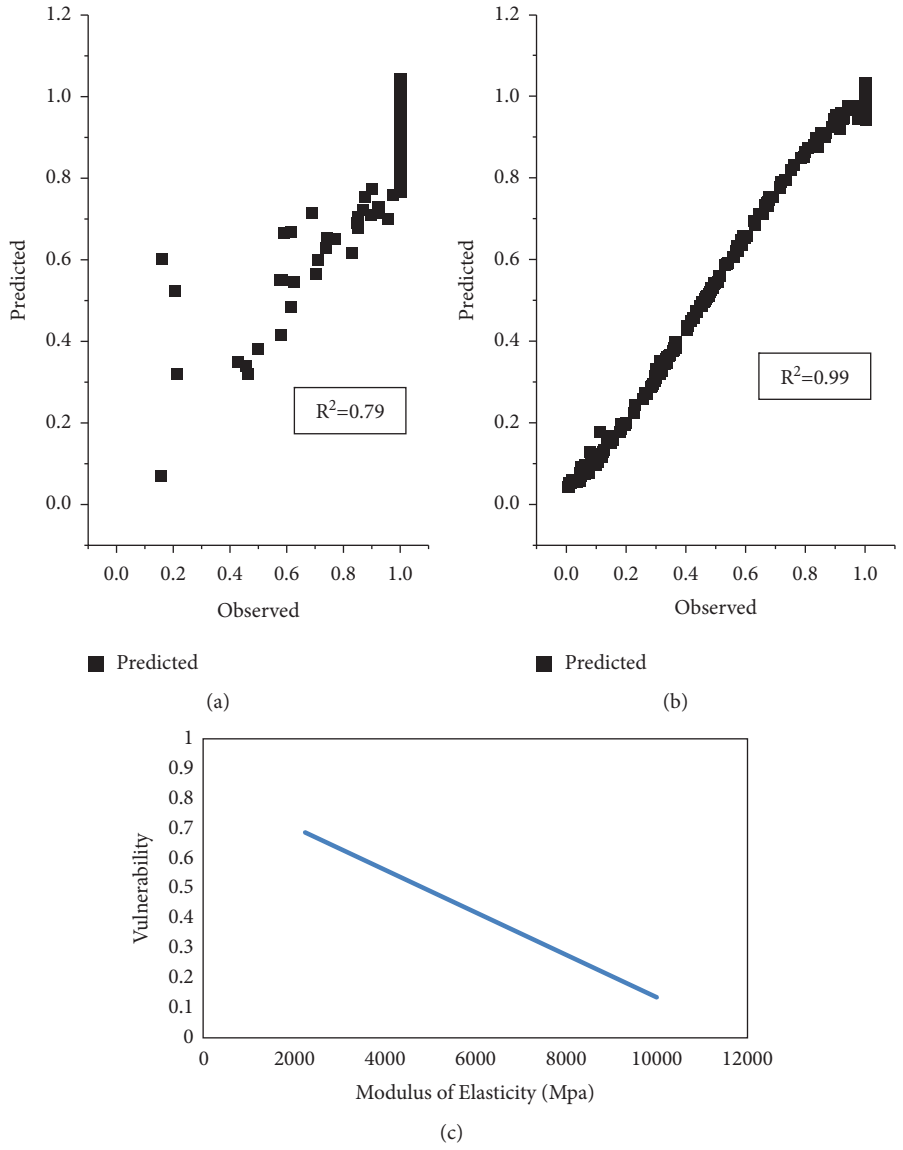

Figure 16: SVM model. (a, b) Performance of testing dataset of $E = 2{,}250$ MPa and 10,000 MPa. (c) Variation of the vulnerability of the building for modulus of elasticity.

accuracy of 0.93 in training and 0.79 in testing (Figures 16(a) and 16(b)). The testing data is less than the training data, which shows that the SVM model does not overfit the model and helps in attaining valuable predictions [57]. The input parameters such as the lateral Earth thrust and the angle of inclination of the building are calculated from the finite element analysis. The length and the width of the building are set as 15 m and 10 m for the analysis. The elastic modulus of the building is set for the masonry building parameters. Table 3 shows the parameters used for the model. The tests were carried out to find the performance of the building when they have different heights and elastic modulus of the building.

The test was conducted to find the efficiency in the material properties ($E = 10000$ MPa) and R^2 accuracy of the building performance is found to be 0.99 for both training and testing (Figures 16(a) and 16(b)). The modulus of elasticity of RCC is considered to study the vulnerability of the building. The results showed that the vulnerability of the building decreased due to the increased material properties with all other properties being the same as before iteration.

Reference [70] provides guidelines for the selection of the site for buildings in the hilly region. The building considered in this study was built at a distance of 3 m from the vertical cut. The vertical cut height is 11 m, which is more than the codal provisions and, hence, is not safe. The building had a height of 4 m and the lateral thrust force acting on the wall is 1200 kN/m^2. The vulnerability according to equation (4) shows the vulnerability is 1. Figure 16(c) shows the relation between vulnerability and elastic properties of the building. It shows the vulnerability value of different building elastic properties ranging from 2250 MPa to 10000 MPa. The building height considered for the analysis is 3 m and the lateral thrust acting on the

Table 3: Parameters used in the model.

Parameters	Unit	Range
Lateral Earth thrust (q)	kN/m^2	0 to 1200
Height of the building (H)	m	3
Length of the building (L)	m	15
Width of the building (W)	m	10
Elastic modulus (E)	MPa	2250 to 10000
Ratio of inclination of the building	No unit	0 to 1

building is 300 kN/m^2. The value of vulnerability reduces from 0.7 to 0.3 and the building resistance is increased to 20%. This is the case observed in this study for an inclination value of 0.01. This study shows that proper guidelines are to be framed, designed and the construction of the building should be according to the codal provisions.

8. Conclusions

The numerical investigation and vulnerability analysis of the building failure due to the vertical cut slope failure were carried out. The parameters used for the numerical investigation were obtained from the laboratory investigations and it revealed that the soil along the slip plane is silty sand (SM) and has a very low permeability coefficient. The low permeability of the soil is explained using Field Emission Scanning Electron Microscopy (FE-SEM), Energy-Dispersive X-ray spectrum (EDX), and X-ray diffraction analysis (XRD). FE-SEM images of both soil layers show the presence of kaolinite clay mineral with a large number of pores in it, which is well supported by EDX and XRD. EDX and XRD results indicate the presence of kaolinite clay mineral ($Al_2Si_2O_5(OH)_4$) along with quartz and calcium carbonate ($CaCO_3$) in the topsoil. The presence of calcium carbonate in the soil confirms the weathering process in the soil. The second layer of soil has a significantly less amount of kaolinite clay due to the incomplete weathering process in the soil. Thus, the topsoil experiences a low coefficient of permeability. The reddish colour in the topsoil explains the presence of ferrous content in the soil. The ferrous content helps in the attainment of soil/strength in the dry season due to the formation of ferrous aluminium silicates.

The vertical cut slope failure mechanism is studied based on the transient seepage condition and coupled analysis to identify soil deformation behaviour based on the flow condition. This helps in studying the effect of slope failure in the building. The analysis is carried out by considering the actual rainfall in three stages. The first stage of rainfall is considered from June to July 2018. Results from the first stage revealed that the matric suction of the soil is more and hence there is a negligible displacement in the slope. Analysis results from the second stage of rainfall (1 to 14 August 2018) emphasize the significance of antecedent rainfall in increasing the degree of saturation and pore pressure, thus leading the slope from stable to unstable. The third stage involves heavy rainfall during 15th and 16th of August 2018, with an average rainfall intensity of 187.5 mm/day. The large excess rainfall during the event day increases the pore water pressure and saturation of the soil above the slip surface to 35 kN/m^2 and 80%, respectively. The increase in the saturation of the soil and the reduction in matric suction led to the reduction in the effective stress and shear strength of the soil. Thus, the cut slope failure occurred and damaged the building located nearby. Results from the numerical analysis match reasonably well with the failure pattern observed at the site.

The vulnerability of the building is studied with the physical parameters obtained from the finite element analysis and it is predicted using the Support Vector Method of regression. The testing data showed that the predicted value and the observed value of vulnerability fitted very efficiently. The values showed the importance of the material properties in the increase in building resistance to 20%. This showed there should be proper guidelines and the building should be built according to codal provisions to avoid such a failure in the future.

Any one of the vertical cut stabilization measures needs to be considered before the construction of a building near the vertical cut. Soil nailing, Reinforced Earth (RE) walls, and slope stabilizing piles are useful stabilization measures.

Data Availability

Necessary data are included in the manuscript.

Conflicts of Interest

The authors declare that they have no conflicts of interest regarding the publication of this paper.

References

[1] P. R. Orense, S. Shimoma, K. Maeda, and I. Towhata, "Instrumented model slope failure due to water seepage," *Journal of Natural Disaster Science*, vol. 26, no. 1, pp. 15–26, 2004.

[2] D. Petley, "Global patterns of loss of life from landslides," *Geology*, vol. 40, no. 10, pp. 927–930, 2012.

[3] D. B. Kirschbaum, R. Adler, Y. Hong, S. Hill, and A. Lerner-Lam, "A global landslide catalog for hazard applications: method, results, and limitations," *Natural Hazards*, vol. 52, no. 3, pp. 561–575, 2010.

[4] D. Kirschbaum and T. Stanley, "Satellite-based assessment of rainfall-triggered landslide hazard for situational awareness," *Earth's Future*, vol. 6, no. 3, pp. 505–523, 2018.

[5] T. H. Nilsen and B. L. Turner, *Influence of Rainfall and Ancient Landslide Deposits on Recent Landslides (1950-71) in Urban Areas of Contra Costa County*, California, California, USA, 1975.

[6] R. H. Campbell, *Soil Slips, Debris Flows, and Rainstorms in the Santa Monica Mountains and Vicinity*, southern California, California, USA, 1975.

[7] S. A. Anderson and N. Sitar, "Analysis of rainfall-induced debris flows," *Journal of Geotechnical Engineering*, vol. 121, pp. 544–552, 1995.

[8] R. M. Iverson, M. E. Reid, and R. G. LaHusen, "Debris-flow mobilization from landslides," *Annual Review of Earth and Planetary Sciences*, vol. 25, no. 1, pp. 85–138, 1997.

[9] S. S. Chandrasekaran, R. Sayed Owaise, S. Ashwin, R. M. Jain, S. Prasanth, and R. B. Venugopalan, "Investigation on infrastructural damages by rainfall-induced landslides during

November 2009 in Nilgiris, India," *Natural Hazards*, vol. 65, no. 3, pp. 1535–1557, 2013.

[10] S. Vadivel and C. S. Sennimalai, "Failure mechanism of long-runout landslide triggered by heavy rainfall in achanakkal, nilgiris, India," *Journal of Geotechnical and Geoenvironmental Engineering*, vol. 145, Article ID 04019047, 2019.

[11] V. Senthilkumar, S. S. Chandrasekaran, and V. B. Maji, "Geotechnical characterization and analysis of rainfall-induced 2009 landslide at Marappalam area of Nilgiris district, Tamil Nadu state, India," *Landslides*, vol. 14, no. 5, pp. 1803–1814, 2017.

[12] V. Senthilkumar, S. S. Chandrasekaran, and V. B. Maji, "Rainfall-induced landslides: case study of the marappalam landslide, nilgiris district, Tamil nadu, India," *International Journal of Geomechanics*, vol. 18, pp. 1–13, 2018.

[13] R. Andrewwinner and S. S. Chandrasekaran, "Investigation on the failure mechanism of rainfall-induced long-runout landslide at Upputhode, Kerala state of India," *Land*, vol. 10, no. 11, p. 1212, 2021.

[14] D C. Brain and Z. Dobroslav, "Stability analyses of rainfall induced landslides," *Journal of Geotechnical and Geoenvironmental Engineering*, vol. 130, pp. 362–372, 2004.

[15] G. Wang and K. Sassa, "Factors affecting rainfall-induced flowslides in laboratory flume tests," *Géotechnique*, vol. 51, no. 7, pp. 587–599, 2001.

[16] H. ., D. G. Fredlund Rahardjo, *Soil Mechanics for Unsaturated Soils*, Wiley, New Jersey, USA, 1993.

[17] H. Rahardjo, T. T. Lim, M. F. Chang, and D. G. Fredlund, "Shear-strength characteristics of a residual soil," *Canadian Geotechnical Journal*, vol. 32, no. 1, pp. 60–77, 1995.

[18] S. L. Kuriakose, S. Devkota, D. G. Rossiter, and V. G. Jetten, "Prediction of soil depth using environmental variables in an anthropogenic landscape, a case study in the Western Ghats of Kerala, India," *Catena*, vol. 79, no. 1, pp. 27–38, 2009.

[19] K. S. Sajinkumar, S. Anbazhagan, A. P. Pradeepkumar, and V. R. Rani, "Weathering and landslide occurrences in parts of Western Ghats, Kerala," *Journal of the Geological Society of India*, vol. 78, no. 3, pp. 249–257, 2011.

[20] T. R. Martha, P. Roy, K. Khanna, K. Mrinalni, and K. Vinod Kumar, "Landslides mapped using satellite data in the Western Ghats of India after excess rainfall during August 2018," *Current Science*, vol. 117, no. 5, pp. 804–812, 2019.

[21] K. M. R. Hunt and A. Menon, "The 2018 Kerala floods: a climate change perspective," *Climate Dynamics*, vol. 54, no. 3-4, pp. 2433–2446, 2020.

[22] IMD, *Malappuram District Rainfall for Last Five Years* , vol. 25, Accessed, Oct, 2018.

[23] D. Varnes, "Landslide hazard zonation: a review of principles and practice," *Natural Hazards*, vol. 3, no. 19, p. 63, 1984.

[24] *UNDRO UNDRO News*, UNDRO, PP ,Geneva : Geneva, July/Aug. 1984.

[25] C. J. van Westen, T. W. J. van Asch, and R. Soeters, "Landslide hazard and risk zonation-why is it still so difficult?" *Bulletin of Engineering Geology and the Environment*, vol. 65, no. 2, pp. 167–184, 2006.

[26] C. N. Subasinghe and A. Kawasaki, "Assessment of physical vulnerability of buildings and socio-economic vulnerability of residents to rainfall induced cut slope failures: a case study in central highlands, Sri Lanka," *International Journal of Disaster Risk Reduction*, vol. 65, Article ID 102550, 2021.

[27] Q. Chen, L. Chen, L. Gui et al., "Assessment of the physical vulnerability of buildings affected by slow-moving landslides," *Natural Hazards and Earth System Sciences*, vol. 20, no. 9, pp. 2547–2565, 2020.

[28] The HINDU, "Rain continues to pound Malappuram," https://www.thehindu.com/news/national/kerala/rain-continues-to-pound-malappuram/article24696358.ece.

[29] S. L. Kuriakose, V. G. Jetten, C. J. van Westen, G. Sankar, and L. P. H. van Beek, "Pore water pressure as a trigger of shallow landslides in the western Ghats of Kerala, India: some preliminary observations from an experimental catchment," *Physical Geography*, vol. 29, no. 4, pp. 374–386, 2008.

[30] "GSI," *GSI Available Online*, May 10, 2020.

[31] K. S. Akhil and D. Venkat Reddy, "Geological and Geotechnical Investigations of Calicut Granite of Kerala State - A Case in Study," in *Proceedings of the National Conference on Technological Innovations for Sustainable infrastructure*, Calicut, India, March 2015.

[32] M. R. Mitchell, R. E. Link, O. F. Usluogullari, and C. Vipulanandan, "Stress-strain behavior and California bearing ratio of artificially cemented sand," *Journal of Testing and Evaluation*, vol. 39, no. 4, pp. 103165–6103645, 2011.

[33] "PLAXIS-3D CONNECT edition V21.01," *PLAXIS 3D-Reference Manual*, pp. 1–600, 2021.

[34] D. Kyung and J. Lee, "Interpretative analysis of lateral load-carrying behavior and design model for inclined single and group micropiles," *Journal of Geotechnical and Geoenvironmental Engineering*, vol. 144, pp. 1–11, 2018.

[35] M. T. van Genuchten, "A closed-form equation for predicting the hydraulic conductivity of unsaturated soils," *Soil Science Society of America Journal*, vol. 44, no. 5, pp. 892–898, 1980.

[36] R. D. Hart, C. L. Detournay, and P. A. Cundall, "Continuum and distinct element modeling in geo-engineering," in *Proceedings of the Proceedings First FLAC/DEM Symposium*, vol. 25, MN, USA, 2008.

[37] J. Bear, *Hydraulics of Groundwater*, McGraw-Hill Book Co., New York, 1979.

[38] F. J. Leij, "The UNSODA unsaturated soil hydraulic database: user's manual," *National Risk Management Research Laboratory, Office of Research and*, vol. 96, 1996.

[39] J. H. M. Wösten and M. T. van Genuchten, "Using texture and other soil properties to predict the unsaturated soil hydraulic functions," *Soil Science Society of America Journal*, vol. 52, no. 6, pp. 1762–1770, 1988.

[40] M. Alam, O. Chaallal, and B. Galy, "Flexible temporary shield in soft and sensitive clay: 3D FE modelling of experimental field test," *Modelling and Simulation in Engineering*, vol. 2021, pp. 1–15, Article ID 6626750, 2021.

[41] M. Papathoma-Köhle, "Vulnerability curves vs. vulnerability indicators: application of an indicator-based methodology for debris-flow hazards," *Natural Hazards and Earth System Sciences*, vol. 16, no. 8, pp. 1771–1790, 2016.

[42] M. Silva and S. Pereira, "Assessment of physical vulnerability and potential losses of buildings due to shallow slides," *Natural Hazards*, vol. 72, no. 2, pp. 1029–1050, 2014.

[43] M. Papathoma-Köhle, B. Neuhäuser, K. Ratzinger, H. Wenzel, and D. Dominey-Howes, "Elements at risk as a framework for assessing the vulnerability of communities to landslides," *Natural Hazards and Earth System Sciences*, vol. 7, no. 6, pp. 765–779, 2007.

[44] A. Puissant, M. Van Den Eeckhaut, M. Kappes et al., "Index-oriented methodologies for landslide consequence analysis: an application to a mountain community in the French alps," in *Landslide Science and Practice: Volume 7: Social and Economic IMPact and Policies*, C. Margottini, P. Canuti, and K. Sassa, Eds., vol. 18, pp. 159–167, Springer, Berlin, Heidelberg, 2013.

[45] J. B. Burland and C. P. Wroth, "Settlement of buildings and associated damage," in *Proceedings of the Settlement of Structures, Proceedings of the Conference of the British Geotechnical Society*, pp. 611–654, Hertsford, England, January 1975.

[46] S. P. Timoshenko, *Strength of Materials Pt. 1, Pt. 1*, Van Nostrand, New York, USA, 1955.

[47] J. B. G. A. Calejo, *3d Modelling of Sheet Pile Corner in Difficult Ground Conditions*, Universidade Do Porto, Porto, Portugal, 2015.

[48] C. Tarbotton, F. Dall'Osso, D. Dominey-Howes, and J. Goff, "The use of empirical vulnerability functions to assess the response of buildings to tsunami iMPact: CoMParative review and summary of best practice," *Earth-Science Reviews*, vol. 142, 2015.

[49] H.-s. Kang and Y.-t. Kim, "The physical vulnerability of different types of building structure to debris flow events," *Natural Hazards*, vol. 80, no. 3, pp. 1475–1493, 2016.

[50] C. Chiocchio, G. Iovine, and M. Parise, "A proposal for surveying and classifying landslide damage to buildings in urban areas," *Eng. Geol. Environ. Proc. sympsium, Athens, 1997*, vol. 1, no. 1997, pp. 553–558, 1977.

[51] A. H. Cooper, "The classification, recording, databasing and use of information about building damage caused by subsidence and landslides," *The Quarterly Journal of Engineering Geology and Hydrogeology*, vol. 41, no. 3, pp. 409–424, 2008.

[52] Y. B. Dibike, S. Velickov, D. Solomatine, and M. B. Abbott, "Model induction with support vector machines: introduction and applications," *Journal of Computing in Civil Engineering*, vol. 15, 2001.

[53] T. Asefa, M. W. Kemblowski, G. Urroz, M. McKee, and A. Khalil, "Support vectors-based groundwater head observation networks design," *Water Resources Research*, vol. 40, no. 11, 2004.

[54] X. Zhang, R. Srinivasan, and M. Van Liew, "Approximating SWAT model using artificial neural network and support vector machine," *JAWRA Journal of the American Water Resources Association*, vol. 45, no. 2, pp. 460–474, 2009.

[55] V. Budamala and A. B. Mahindrakar, "Adaptive hybrid architecture for enhancement of the complex hydroclimatic system and assessment of freshwater security," *Journal of Hydroinformatics*, vol. 23, no. 5, pp. 950–965, 2021.

[56] V. Budamala and A. Baburao Mahindrakar, "Enhance the prediction of complex hydrological models by pseudo-simulators," *Geocarto International*, vol. 36, no. 9, pp. 1027–1043, 2021.

[57] P. Samui, "Slope stability analysis: a support vector machine approach," *Environmental Geology*, vol. 56, no. 2, pp. 255–267, 2008.

[58] "ASTM D2487-11," in *Proceedings of the Standard Practice for Classification of Soils for Engineering Purposes (Unified Soil Classification System)*, p. 5, American Society for Testing Materials, 2011.

[59] *IS2720(17) Indian Standard Methods of Tests for Soils: Laboratory Determination of Permeability Bur*, Indian Stand., New Delhi, 1986.

[60] P. Samui, "Slope stability analysis: A support vector machine approach. Environ," *Geol*, vol. 56, pp. 255–267, 2008.

[61] ASTM D2487-11, *Proceedings of the Standard Practice for Classification of Soils for Engineering Purposes (Unified Soil Classification System)*, American Society for Testing and Materials, West Conshohocken, PA, USA, 2011.

[62] IS2720 Part-17, *Indian Standard Methods of Tests for Soils: Laboratory Determination of Permeability*, Bureau of Indian Standards, New Delhi, India, 1986.

[63] B. F. Mallory and D. N. Cargo, *Physical Geology*, Article ID 007085047X, 1979.

[64] "BS5930-1999 Code of practice for site investigations (formerly CP 2001)," *International Journal of Rock Mechanics and Mining Science & Geomechanics Abstracts*, vol. 18, p. 106, 1981.

[65] "Weathering of rocks," *Developments in Geotechnical Engineering*, vol. 10, pp. 146–162, 1976.

[66] K. S. Sajinkumar and S. Anbazhagan, "Geomorphic appraisal of landslides on the windward slope of Western Ghats, southern India," *Natural Hazards*, vol. 75, no. 1, pp. 953–973, 2015.

[67] J. L. R. Touret and J. M. Huizenga, "Charnockite microstructures: from magmatic to metamorphic," *Geoscience Frontiers*, vol. 3, no. 6, pp. 745–753, 2012.

[68] "GSI Systematic geological mapping and preliminary mineral investigation in parts of Kozhikode taluk, Kozhikode district,Manjeri and Tirur taluks," *Malappuram district, Kerala state*, vol. 5973, pp. 1–23, 1973.

[69] M. E. José and H. Laureano, "Effect of degree of weathering on dynamic properties of residual soils," *J. Geotech. Eng*, vol. 122, pp. 988–997, 1996.

[70] *IS14243-2 Guidelines For Selection and Development of Site for Building in hill Areas*, Part 2: Selection and development, 1995.